JOURNAL OF SYNCHROTRON RADIATION
ISSN 1600-5775

Thickness of carbon coatings on silicon materials determined by hard X-ray photoelectron spectroscopy at multiple photon energies

Noritake Isomura,* Naoko Takahashi, Satoru Kosaka and Hiroyuki Kawaura

Toyota Central R&D Laboratories, Inc., 41-1 Yokomichi, Nagakute, Aichi 480-1192, Japan.
*Correspondence e-mail: isomura@mosk.tytlabs.co.jp

Received 8 July 2019
Accepted 6 August 2019

Edited by S. Svensson, Uppsala University, Sweden

Keywords: hard X-ray photoelectron spectroscopy (HAXPES); lithium-ion battery (LIB); silicon negative electrodes; layered polysilane; carbon coating.

Hard X-ray photoelectron spectroscopy at multiple photon energies is used to investigate the surface structure of carbon coatings on silicon materials destined for use as negative electrodes in lithium-ion batteries. The photoelectron intensity from the carbon coatings decreases with an increase in the kinetic energy of the photoelectron. By fitting the photoelectron intensity versus energy to numerically derived curves, the thickness and coverage of the carbon coatings can be obtained. The results are in agreement with the values suggested by the cross-sectional secondary-electron microscopy images of the carbon coatings, although the thickness should be corrected by accounting for the rectangular parallelepiped structure of the silicon material.

1. Introduction

Owing to the widespread and growing use of electric vehicles, notebook computers and mobile phones, among others, the demand for lithium-ion batteries (LIBs) has increased (Lu *et al.*, 2013). Although graphite is often used in negative LIB electrodes, it has the disadvantage of low-energy capacity (372 mA h g^{-1}) (Winter *et al.*, 1998). Silicon has a high theoretical energy capacity of 4200 mA h g^{-1} (Chan *et al.*, 2008) which is over an order of magnitude greater than the energy capacity of graphite and is expected to be used as a material for negative electrodes in next-generation LIBs.

To increase the conductivity, carbon coatings are deposited on the surface of Si electrodes and range in thickness from nanometres to tens of nanometres (Fu *et al.*, 2013; Li *et al.*, 2014; Yang *et al.*, 2015). Fu *et al.* (2013) reported that the addition of a C coating improves the capacity and cyclic stability of a device. As may be expected, the thickness of such C coatings increases (10–17 nm) with increasing deposition time, and the cyclic energy capacity varies between samples subjected to different C-deposition times. For example, herein, a thin 10 nm C coating is nonuniform. These results show that the thickness and uniformity of the C coating affects the energy capacity and therefore can be key factors in the Si electrode.

The surface states of Si electrodes have been investigated using hard X-ray photoelectron spectroscopy (HAXPES) (Philippe *et al.*, 2012; Young *et al.*, 2015). The analysis depth of HAXPES ranges from nanometres to tens of nanometres (Powell & Tanuma, 2015), making it appropriate for analyzing C coatings because the coating thickness is roughly the same order of magnitude as the analysis depth. In general, the thickness of coatings on flat surfaces is determined by angle-resolved measurements (Kimura *et al.*, 2008) because surface

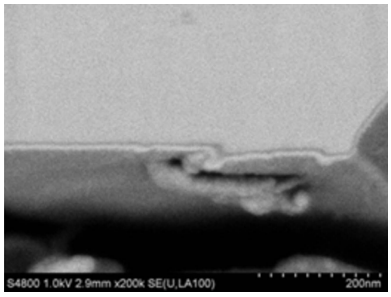

smoothness is crucial for such measurements (Merzlikin *et al.*, 2008). However, these measurements cannot be applied to LIB electrodes because their surfaces are covered with particles or flakes, which create bumps and dips on the surface.

To overcome this drawback, we present herein a modified surface-structure analysis technique based on HAXPES with multiple photon energies (PEs) (Isomura *et al.*, 2015, 2016). The distinguishing aspect of this technique is that the detector (electron analyzer) is placed normal to the sample surface, allowing detection of electrons emitted from surfaces with bumps and dips, in contrast to angle-resolved measurements that detect photoelectrons emitted at small angles, which leads to shadows from the bumps and dips. However, the depth resolution is reduced because the rough surfaces lead to various electron-emission angles, even for detection normal to the sample surface.

We use the modified HAXPES method to measure the coating thickness and coverage of a multilayer sample (Au/SiO_2/Si) whose top (Au) layer has an island-like structure which we model as bumps and dips. The analysis depth corresponds to the electron inelastic mean free path (IMFP), which depends on the kinetic energy of the emitted electrons that in turn is relatively high because of the high photon energy used in the HAXPES technique (Tanuma *et al.*, 2011). Thus, varying the energy of the incident photons allows measurements of varying analysis depths.

Thus, motivated by the desire to improve the performance of the negative electrode of LIBs, we use HAXPES with multiple PEs to analyze the surface structure of the Si electrode sample and hence investigate the structure of C coatings on Si. The thickness and coverage of C coatings on Si are determined from fitting curves of intensity versus energy of emitted photoelectrons.

2. Experimental

The experiments were performed at the BL6N1 beamline of the Aichi Synchrotron Radiation Center (AichiSR) for a PE of 3 keV and at the BL46XU beamline of Super Photon Ring 8 GeV (SPring-8) for PEs of 6 keV, 8 keV and 10 keV. Details of the beamlines have been given elsewhere (Yamamoto *et al.*, 2014; Yasuno *et al.*, 2016).

AichiSR has a 72 m-circumference electron storage ring and is operated at 1.2 GeV electron energy and 300 mA current. White light from a bending magnet was monochromated by an InSb(111) double-crystal monochromator. The beam size at the sample position was 3.5 mm × 2 mm (horizontal × vertical). The electron analyzer (PHOIBOS 150, SPECS GmbH) consisted of a hemispherical energy analyzer with a mean radius of 150 mm. The pass energy was 20 eV and the total energy resolution was 1.0 eV. The X-ray beam from the beamline was horizontally polarized. The axis of the input lens of the analyzer was also horizontal, and the angle between the axis and the incident beam was 54°. The take-off angle of the analyzed electrons was set to 90° (normal to the sample surface). The base pressure of the main chamber was approximately 5×10^{-8} Pa.

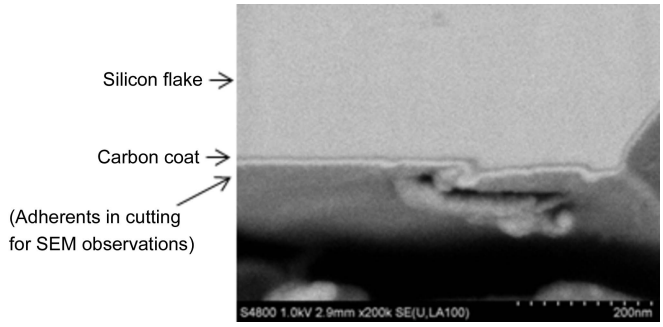

Figure 1
Cross-sectional SEM image of an Si flake with C coating.

SPring-8 has a 1436 m-circumference electron storage ring and is operated at 8 GeV electron energy and 100 mA current. Quasi-monochromatic light from an undulator was monochromated by an Si(111) double-crystal monochromator followed by an Si channel-cut monochromator. The beam size at the sample position was 0.2 mm × 0.02 mm (horizontal × vertical). The electron analyzer (R4000, Scienta Omicron GmbH) consisted of a hemispherical energy analyzer with a mean radius of 200 mm. The pass energy was 200 eV and the total energy resolution was 0.25 eV. The lens axis of the analyzer was oriented perpendicular to the incident X-ray beam and parallel to the polarization vector. The incidence angle relative to the sample surface was set to 10° and the take-off angle of the analyzed electrons was 80°. The base pressure of the main chamber was approximately 1×10^{-6} Pa.

The sample consisted of flakes of layered polysilane of an average size of ∼5 µm (hereafter, Si flakes) coated with C. The Si flakes were synthesized by reacting $CaSi_2$ with aqueous HCl at −30°C, as per Kumai & Nakano (2015). The C was deposited by 2 h of chemical vapor deposition using the thermal decomposition of C_2H_2 as the C precursor gas at 1000°C, as per Fu *et al.* (2013). For the HAXPES measurements, the sample was embedded in an indium sheet that contained no Si or C. Secondary-electron microscopy (SEM) was used to acquire cross-sectional images of the sample in a plane cut by cross-section polisher using argon ions and observed at 1 kV using field-emission SEM (S-4800, Hitachi) (Fig. 1). The resulting image reveals that a uniform C coating 4–8 nm-thick (6 nm on average) forms on the Si flakes. Because the photoionization cross section depends on the PE and the angular distribution of emitted electrons (Isomura *et al.*, 2014) varies between synchrotron facilities, we used a highly oriented pyrolytic graphite (HOPG) substrate as a bulk C standard to calibrate the C 1*s* photoelectron intensity at each PE.

3. Results and discussion

Fig. 2 shows the HAXPES spectra from C-coated Si flakes obtained at multiple PEs. At each PE, the Si 1*s* spectral peaks at 1839.5 eV and 1844.5 eV are assigned to Si and SiO_2, respectively (Walsh *et al.*, 2012). The peak intensity ratio of SiO_2 to Si is largest for a PE of 3 keV, and decreases with increasing PE, although it is almost the same for the PEs of

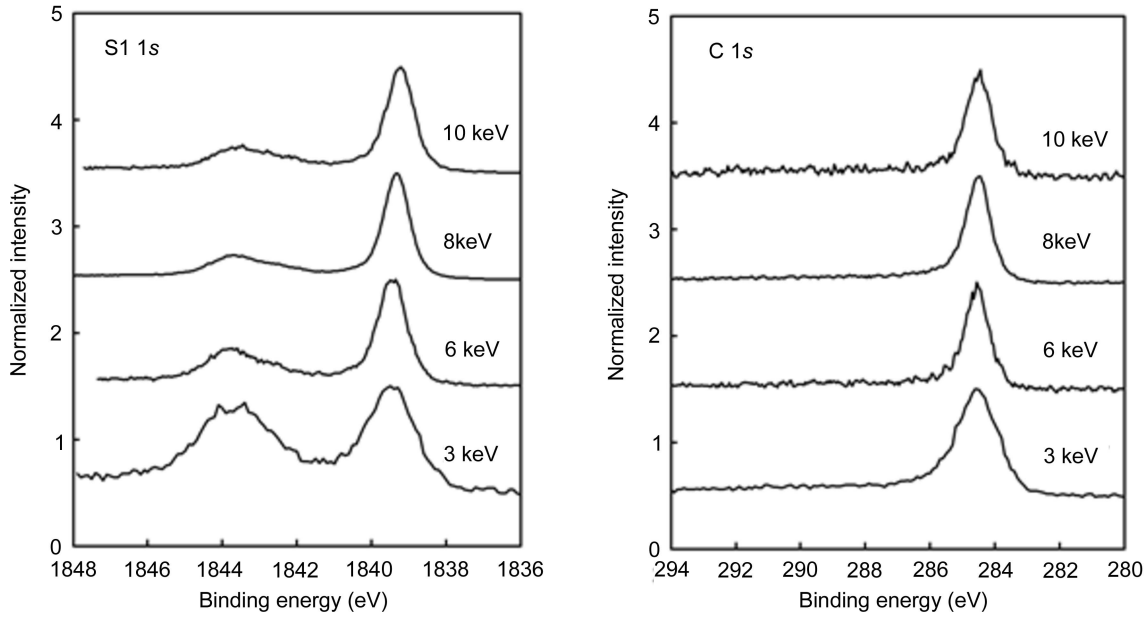

Figure 2
HAXPES spectra from Si flakes with C coatings, obtained at the photon energies indicated for each spectrum.

8 keV and 10 keV. This result suggests that SiO_2 may be present at the surface of the Si flakes (*i.e.* at the interface between the C coating and the Si flake) because the contribution of the surface region becomes distinct due to the shorter IMFP at lower PE [in SiO_2, the IMFP is 5.5 nm, 7.6 nm, 10.5 nm and 13.4 nm at 3 keV, 6 keV, 8 keV and 10 keV, respectively (Tanuma *et al.*, 2011)]. The presence of SiO_2 is consistent with the oxidization of layered polysilane to SiO_2 described by Kumai & Nakano (2015). There is a C 1*s* spectral peak at 284.5 eV for each PE, and these peaks are assigned to graphite (Yamamoto *et al.*, 1998). This C 1*s* peak represents the state of the entire C coating because the incident X-rays penetrate through the C coating, as testified by the Si 1*s* spectra from the Si flakes beneath the C coating. In addition, no peaks appear from the indium in the indium sheet.

Fig. 3 shows the simulated C 1*s* photoelectron intensities as a function of kinetic energy of photoelectrons as a result of C coatings of varying thickness and coverage. The simulation method is described in detail elsewhere (Isomura *et al.*, 2015). In brief, the intensity I_i and concentration $X_i(z)$ of photoelectrons from element i are described by the following function of the electron escape depth (Hofmann, 1983),

$$\frac{I_i}{I_i^0} = \frac{1}{\lambda_i}\int_0^\infty X_i(z)\exp(-z/\lambda_i)\,\mathrm{d}z, \qquad (1)$$

where I_i^0 is the intensity from an elemental bulk standard, λ_i is the 'effective' escape depth of the photoelectrons and $X_i(z)$ is the concentration of element i at depth z. The effective escape depth λ_i is determined from the normal component of the IMFP for a given energy and material. The IMFPs for the various PEs are obtained by using the algorithm of Tanuma, Powel and Penn (TPP-2M) (Tanuma *et al.*, 2011) and are integrated over the appropriate fraction of covered and non-covered regions.

In Fig. 3, the photoelectron intensity gradually decreases with increasing energy. The photoelectron intensity increases as the C coat becomes thicker and is relatively large at low energy with greater coverage. By using this simulation, the thickness and coverage of the C coating are determined by fitting the photoelectron intensity versus energy.

Fig. 4 shows the measured C 1*s* photoelectron intensities from the C coating as a function of kinetic energy of a photoelectron. The photoelectron intensity is defined as the ratio of the area under the peak to that under the same peak in the calibration sample (HOPG), and the Shirley method was used to subtract the background (Shirley, 1972). The photoelectron intensity decreases gradually with increasing energy, which is consistent with the simulation result (Fig. 3). The

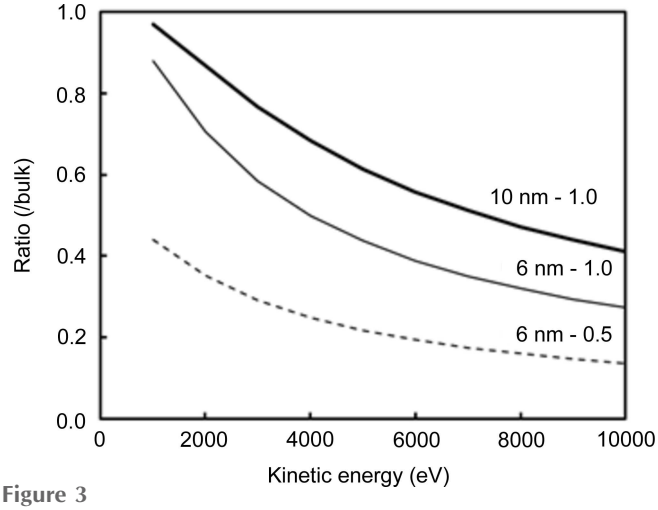

Figure 3
Simulated C 1*s* photoelectron intensity as a function of kinetic energy of a photoelectron and for the C-coating thicknesses and coverages indicated above each curve. The photoelectron intensity is defined as the ratio of the area under the peak to that under the same peak in the calibration sample (HOPG).

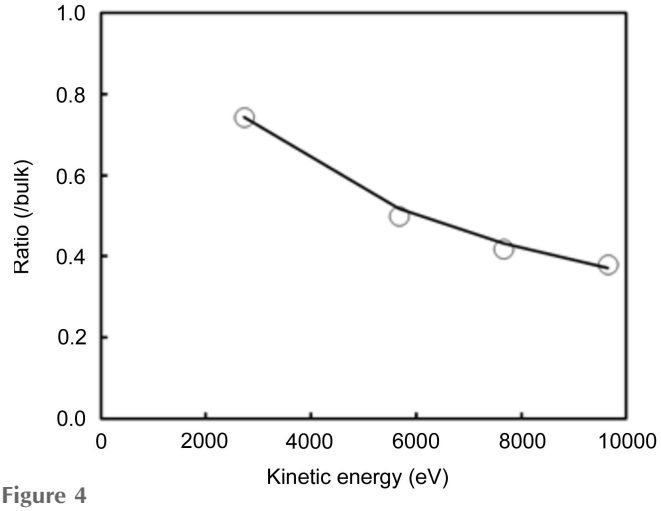

Figure 4
Measured result of C 1*s* photoelectron intensity as a function of kinetic energy of the photoelectrons (circles). The line is a least-squares fit to equation (1).

measured data were fit by using a least-squares approximation to obtain the thickness and coverage of the C coating. The fit is consistent with the experimental result, as shown in Fig. 4, and gives a thickness and coverage of 8.4 nm and 1.0, respectively. A coverage of 1.0 means that the C coating has uniform thickness, which is consistent with the SEM image (Fig. 1). Conversely, a thickness of 8.4 nm is 40% greater than the thickness of 6 nm obtained from the cross-sectional SEM observations. The Si flakes are rectangular, randomly oriented parallelepipeds with flat surfaces (Fig. 1). Thus, the surfaces may be regarded as faces slanted at 45° on average, resulting in an apparent thickness of $\sqrt{2} \simeq 1.4$ times the actual thickness of the Si flakes, which is consistent with the value obtained by fitting the energy dependence.

4. Conclusions

We analyze the surface structure of C coatings on Si flakes by using HAXPES at multiple PEs. The photoelectron intensity from the C coating gradually decreases with increasing kinetic energy of the photoelectron. By fitting simulations to the measured photoelectron intensity versus energy, we obtain 8.4 nm and 1.0 as the thickness and surface coverage of the C coating, respectively. A coverage of 1.0 means that the C coating has uniform thickness. A thickness of 8.4 nm is consistent with a thickness of 6 nm obtained from cross-sectional SEM images if we consider the random orientation of rectangular parallelepiped Si flakes with flat surfaces. These results demonstrate that the states of C coatings formed on Si can be evaluated nondestructively by applying HAXPES at multiple PEs to analyze the surface structure analysis. Such analyses are important for improving LIB negative electrodes.

Acknowledgements

The authors are grateful to Dr Hiroshi Oji of AichiSR and Dr Satoshi Yasuno of SPring-8 for their help in the HAXPES measurements. The synchrotron radiation measurements were performed at BL6N1 of AichiSR and BL46XU of SPring-8.

References

Chan, C. K., Peng, H., Liu, G., McIlwrath, K., Zhang, X. F., Huggins, R. A. & Cui, Y. (2008). *Nat. Nanotechnol.* **3**, 31–35.
Fu, K., Xue, L., Yildiz, O., Li, S., Lee, H., Li, Y., Xu, G., Zhou, L., Bradford, P. D. & Zhang, X. (2013). *Nano Energy*, **2**, 976.
Hofmann, S. (1983). *Practical Surface Analysis*, p. 141, edited by D. Briggs & M. P. Seah. Chichester: John Wiley.
Isomura, N., Kataoka, K., Horibuchi, K., Dohmae, K., Oji, H., Cui, Y.-T., Son, J.-Y., Kitazumi, K., Takahashi, N. & Kimoto, Y. (2015). *Surf. Interface Anal.* **47**, 265–269.
Isomura, N., Kataoka, K., Horibuchi, K., Dohmae, K., Oji, H., Cui, Y.-T., Son, J.-Y., Kitazumi, K., Takahashi, N. & Kimoto, Y. (2016). *AIP Conf. Proc.* **1741**, 050015.
Isomura, N., Kitazumi, K., Kataoka, K., Takahashi, N., Kimoto, Y. & Dohmae, K. (2014). *J. Electron Spectrosc. Relat. Phenom.* **195**, 62–65.
Kimura, K., Nakajima, K., Zhao, M., Nohira, H., Hattori, T., Kobata, M., Ikenaga, E., Kim, J.-J., Kobayashi, K., Conard, T. & Vandervorst, W. (2008). *Surf. Interface Anal.* **40**, 423–426.
Kumai, Y. & Nakano, H. (2015). *Jpn. J. Appl. Phys.* **54**, 035201.
Li, X., Gu, M., Hu, S., Kennard, R., Yan, P., Chen, X., Wang, C., Sailor, M. J., Zhang, J.-G. & Liu, J. (2014). *Nat. Commun.* **5**, 4105.
Lu, L., Han, X., Li, J., Hua, J. & Ouyang, M. (2013). *J. Power Sources*, **226**, 272.
Merzlikin, S. V., Tolkachev, N. N., Strunskus, T., Witte, G., Glogowski, T., Wöll, C. & Grünert, W. (2008). *Surf. Sci.* **602**, 755–767.
Philippe, B., Dedryvère, R., Allouche, J., Lindgren, F., Gorgoi, M., Rensmo, H., Gonbeau, D. & Edström, K. (2012). *Chem. Mater.* **24**, 1107–1115.
Powell, C. J. & Tanuma, S. (2015). *Hard X-ray Photoelectron Spectroscopy (HAXPES)*, p. 111, edited by J. C. Woicik. Cham: Springer.
Shirley, D. A. (1972). *Phys. Rev. B*, **5**, 4709–4714.
Tanuma, S., Powell, C. J. & Penn, D. R. (2011). *Surf. Interface Anal.* **43**, 689–713.
Walsh, L. A., Hughes, G., Hurley, P. K., Lin, J. & Woicik, J. C. (2012). *Appl. Phys. Lett.* **101**, 241602.
Winter, M., Besenhard, J. O., Spahr, M. E. & Novák, P. (1998). *Adv. Mater.* **10**, 725–763.
Yamamoto, K., Koga, Y., Fujiwara, S., Kokai, F. & Heimann, R. B. (1998). *Appl. Phys. Mater. Sci. Process.* **66**, 115–117.
Yamamoto, M., Yoshida, T., Yamamoto, N., Yoshida, H. & Yagi, S. (2014). *e-J. Surf. Sci. Nanotech.* **12**, 299–303.
Yang, L. Y., Li, H. Z., Liu, J., Sun, Z. Q., Tang, S. S. & Lei, M. (2015). *Sci. Rep.* **5**, 10908.
Yasuno, S., Oji, H., Koganezawa, T. & Watanabe, T. (2016). *AIP Conf. Proc.* **1741**, 030020.
Young, B. T., Heskett, D. R., Nguyen, C. C., Nie, M., Woicik, J. C. & Lucht, B. L. (2015). *Appl. Mater. Interfaces*, **7**, 20004–20011.